Kong et al. Nanoscale Research Letters (2018) 13:80
https://doi.org/10.1186/s11671-018-2488-3

Nanoscale Research Letters

NANO EXPRESS Open Access

Synthesis and Study of Optical Characteristics of $Ti_{0.91}O_2$/CdS Hybrid Sphere Structures

Lingbin Kong, Qinfeng Xu*, Meng Zhang, Dehua Wang, Mingliang Liu, Lei Zhang, Mengmeng Jiao, Honggang Wang and Chuanlu Yang*

Abstract

The optical properties of alternating ultrathin $Ti_{0.91}O_2$ nanosheets and CdS nanoparticle hybrid spherical structures designed by the layer-by-layer (LBL) assembly technique are investigated. From the photoluminescence (PL) spectral measurements on the hybrid spherical structures, a spectrum-shifted fluorescence emission occurs in this novel hybrid material. The time-resolved PL measurements exhibit a remarkably increased PL lifetime of 3.75 ns compared with only $Ti_{0.91}O_2$ spheres or CdS nanoparticles. The novel results were attributed to the enhanced electron-hole separation due to the new type II indirect optical transition mechanism between $Ti_{0.91}O_2$ and CdS in a charge-separated configuration.

Keywords: Hybrid spherical structures, $Ti_{0.91}O_2$ nanosheets, CdS nanoparticles, Indirect optical transitions

Background

Semiconductor composite nanostructures have attracted more attention due to the optimal assembling of conduction band and valance band for the photovoltaic applications and other optoelectronic devices [1–4]. Spatial separation of the electron and hole in the type II semiconductor composite nanostructures can result in a prolonged lifetime of charge carriers which has desirable optical characteristics for applications such as light sources [5, 6], lasers [7–9], and photovoltaic devices [10, 11]. Many studies of indirect optical transition (IOT) effect in the type II composite nanostructures have been reported over the past few years. For instance, IOT phenomenon has been reported in ultrathin hybrid sphere nanostructures including graphene oxide and TiO_2 nanosheets [12] or coupled quantum dots system [13]. In recent years, TiO_2 is an important optical materials which has been widely investigated owing to its outstanding optical properties for use in photocatalysis and solar cells, but the wide bandgap (3.2 eV) of TiO_2 limits its photocatalytic property in the UV region. In order to extensively exploit the optical activity in the visible light region, the surface of TiO_2 nanosheets coated with quantum dots has been investigated as a superior alternative for dye-sensitized solar cell [14–18]. Particularly important, the composite system of TiO_2 nanosheets coupled with CdS quantum dots (QDs) has been widely studied for various applications due to its suitable bandgap (2.4 eV) and excellent optical properties [19–21]. Combining these features, the TiO_2/CdS hybrid structures have been recently highlighted as a unique system [22–26]. Moreover, the CdS nanoparticles coated with TiO_2 nanosheets can greatly improve its optical activity. So far, exciton separation and carrier extraction are the major bottleneck achieving highly efficient material-sensitized solar cells. However, fundamental studies on photoexcited carrier dynamics based on TiO_2/CdS hybrid spheres are limited. Therefore, the photoluminescence (PL) properties and time-resolved PL decays of composite nanostructures consisting of alternating $Ti_{0.91}O_2$ nanosheets and CdS nanoparticles are investigated in this paper. From the PL spectra and time-resolved PL decay measurements, the new type II indirect optical transition contributes to clarify the novel fluorescence emission mechanism of composite nanostructures consisting of $Ti_{0.91}O_2$ nanosheets and CdS nanoparticles that are different from traditional TiO_2/

* Correspondence: xuqf5678@163.com; yangchuanlu@126.com
School of Physics and Optoelectronic Engineering, Ludong University, Yantai 264025, China

CdS fluorescence radiative transition systems. The excitation power- and excitation wavelength-dependent PL spectra and time-resolved PL decay measurements were also further investigated to affirm the recombination properties of charge carriers and elucidate the competition mechanism of different radiative transition pathways in $Ti_{0.91}O_2$/CdS composite nanostructure. These novel results provide a useful viewpoint for the design of charge separation and charge extraction in TiO_2 and CdS composite nanostructures for various optoelectronic device applications.

Methods

Synthesize Samples

The synthesis of $Ti_{0.91}O_2$ nanosheets and CdS nanoparticles has been reported based on the layer-by-layer self-assembly technique [27]. The overall procedure for fabricating multilayer $Ti_{0.91}O_2$/CdS composite nanostructures is demonstrated as follows: the poly(methly methacrylate) (PMMA) solid spheres were completely diluted by the protonic polyethylenimine (PEI) aqueous solution, in order to ensure the saturated adsorption of PEI on PMMA solid spheres surfaces. The PMMA solid spheres coated with PEI are diluted with deionized water by ultrasonic treatment; then, negatively charged $Ti_{0.91}O_2$ nanosheets were added to the hybrid PMMA coated with PEI solution under stirring, the PMMA combine with $Ti_{0.91}O_2$ nanosheets due to the interior electrostatic interaction of the opposite charge. The above procedure was repeated. The multilayer PEI/$Ti_{0.91}O_2$/PEI/CdS hybrid sphere nanostructures that have been deposited onto PMMA spheres were achieved based on the above repeated synthesis procedures. During microwave irradiation, PEI moiety was removed and PMMA particles were decomposed. After reaction, hollow spheres consisting of alternating $Ti_{0.91}O_2$ nanosheets and CdS QDs were obtained, and trifle PMMA residue was removed with tetrahydrofuran (THF). Finally, the hybrid hollow spheres with multilayer $Ti_{0.91}O_2$/CdS nanostructures were obtained.

Experiment Apparatus

The sample images of solid $Ti_{0.91}O_2$/CdS hybrid spheres and hollow $Ti_{0.91}O_2$/CdS hybrid spheres were measured by transmission electron microscopy (TEM) and scanning electron microscopy (SEM), respectively. The appropriate amounts of solid $Ti_{0.91}O_2$/CdS hybrid spheres and hollow $Ti_{0.91}O_2$/CdS hybrid spheres were diluted by deionized water to have lower sample densities. Diluted samples were spin-coated on silica coverslip to prepare thin films for optical measurement with the 266 and 400 nm excitation. The optical measurements of all samples were carried out at room temperature. For PL spectral measurements, the 800 nm ps Ti:Sapphire laser with 76 MHz repetition rate was used to generate the 266 and 400 nm wavelength pulse laser based on second-harmonic and third-harmonic conversion technique, respectively. Two hundred sixty-six nanometer and 400 nm pulse laser at an incident angle of ~ 45° relative to the vertical direction was focused onto the sample surface with a power density of ~ 100 W/cm^2. The PL from samples was collected vertically by a ×60 objective and sent to the spectrometer, and the emission PL spectra were recorded with a monochromator (Acton SP-2500i, 0.5 m, 150 lines mm^{-1} grating, blazed at 500 nm) fitted with a Princeton Instruments liquid-nitrogen-cooled charge-coupled device (CCD) camera. For time-resolved PL decay measurements, the PL from the samples was collected by the same objective and then detected by the single photon counting system with the 250 ps time resolution. Moreover, the corresponding 450, 500, and 550 nm band-pass filter with a 10-nm bandwidth was used to effectively measure the different wavelength PL lifetimes.

Results and Discussion

Figure 1a shows energy levels of $Ti_{0.91}O_2$ nanosheets and CdS nanoparticles, and the CdS nanoparticles have a higher conduction band level compared with that of $Ti_{0.91}O_2$ nanosheets. The scanning electron microscopy (SEM) image of the hybrid spheres $Ti_{0.91}O_2$ nanosheets and CdS nanoparticles with several hundred nanometers length and smooth surfaces are shown in Fig. 1b. The transmission electron microscopy (TEM) images of the solid $Ti_{0.91}O_2$/CdS hybrid spheres and hollow $Ti_{0.91}O_2$/CdS composite sphere nanostructures are shown in Fig. 1c, d, respectively. Figure 1a shows the XRD patterns of pure PMMA, CdS, and $Ti_{0.91}O_2$/CdS film. Compared to pure PMMA, $Ti_{0.91}O_2$/CdS and CdS film exhibits new peaks 2 and 4 indicating the presence of the cubic phase CdS. The composition of $Ti_{0.91}O_2$/CdS was identified by e X-ray photoelectron spectroscopy (XPS), as shown in Fig. 1f. Therefore, hollow spheres consisting of alternating $Ti_{0.91}O_2$ nanosheets and CdS QDs were obtained. In order to further verify synthesis of $Ti_{0.91}O_2$ nanosheets and CdS nanoparticles based on the layer-by-layer self-assembly technique, the absorption spectra and Raman spectra of $Ti_{0.91}O_2$ and $Ti_{0.91}O_2$/CdS are shown in Additional file 1: Figure S1 and Figure S2, respectively. Compared with Raman spectra of $Ti_{0.91}O_2$ nanosheets, the Raman spectra of $Ti_{0.91}O_2$/CdS demonstrate a combination of $Ti_{0.91}O_2$ nanosheets and CdS nanoparticles.

The photoluminescence (PL) spectra of $Ti_{0.91}O_2$ (black), CdS (red), and $Ti_{0.91}O_2$/CdS (black) excited at 266 nm are shown in Fig. 2a. The fluorescence peaks of $Ti_{0.91}O_2$ and CdS are around 450 and 530 nm with the 266 nm excitation, respectively. Because the bandgap

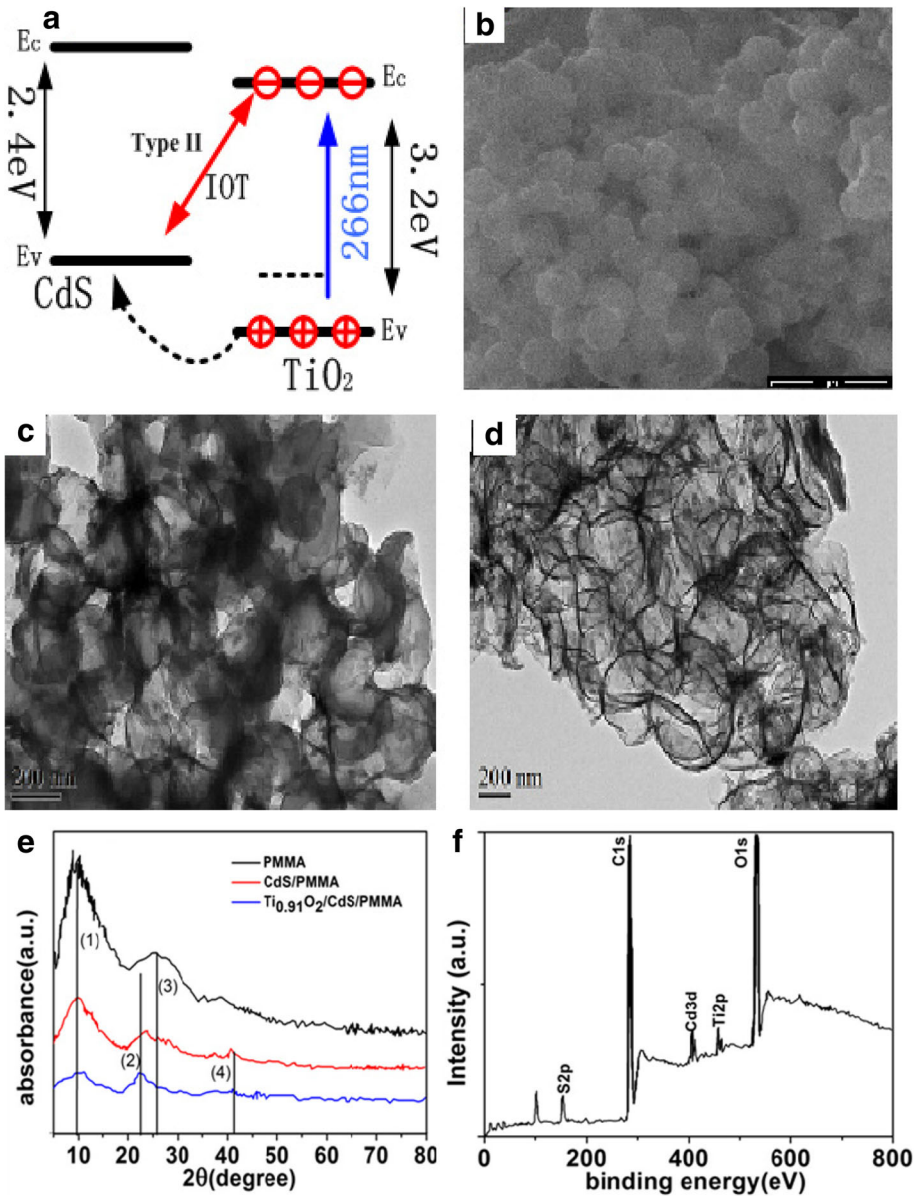

Fig. 1 **a** Energy band diagram of hybrid spheres $Ti_{0.91}O_2$ and CdS. **b** Scanning electron microscopy (SEM) images of $Ti_{0.91}O_2$/CdS. **c** Transmission electron microscopy (TEM) images of the solid $Ti_{0.91}O_2$/CdS hybrid spheres. **d** Hollow $Ti_{0.91}O_2$/CdS hybrid spheres. **e** XRD of PMMA, CdS, and $Ti_{0.91}O_2$/CdS. **f** XPS spectrum of $Ti_{0.91}O_2$/CdS

energy of TiO_2 is 3.2 eV, the red-shifted PL spectra observed in Fig. 2a should attribute to defect levels generated inside the bandgap of $Ti_{0.91}O_2$ so that holes generated in the $Ti_{0.91}O_2$ valence band can relax to different defect state levels by the nonradiative channels and then recombine with the electrons of $Ti_{0.91}O_2$, giving rise to the related defect state optical emission. Under the 266 nm excitation, the fluorescence emission peak around 530 nm from CdS nanoparticles embodies smaller energy bandgap than that of CdS (2.48 eV). We suppose that the nonradiative transition of excited electrons from the conduction band bottom to different defect states level occurs in the CdS nanoparticles. However, the fluorescence emission peak shifts to 500 nm when the $Ti_{0.91}O_2$/CdS hybrid structure excited at 266 nm. If we exclude the contribution of either $Ti_{0.91}O_2$ or CdS to the blue-shifted spectra emission; then, this fluorescence mechanism attributes to an indirect optical transition (IOT) in hybrid interface of $Ti_{0.91}O_2$/CdS system. In the traditional type II TiO_2/CdS composite nanostructure, light excitation of TiO_2 and CdS will transfer electrons from the higher conduction band of CdS to the lower conduction band of TiO_2 and generated holes from the lower value band of TiO_2 to

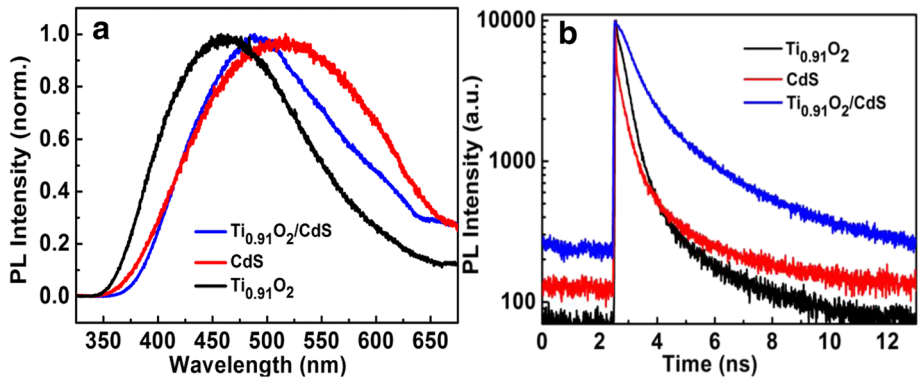

Fig. 2 **a** PL spectra of the $Ti_{0.91}O_2$(black), CdS(red), and $Ti_{0.91}O_2$/CdS (blue) samples excited at 266 nm. **b** PL decay curves of the $Ti_{0.91}O_2$(black), CdS(red), and $Ti_{0.91}O_2$/CdS (blue) samples with the 266 nm excitation

the higher value band of CdS nanoparticles. If the whole PL emission of $Ti_{0.91}O_2$/CdS hollow spheres comes from CdS nanoparticles, we should observe the faster PL decay process caused by a nonradiative decay channel that the electrons transfer from the conduction band of CdS nanoparticles to the conduction band of TiO_2 due to the fluorescence quenching effect as in traditional TiO_2/CdS system. Therefore, a new electron transfer mechanisms were proposed for the present $Ti_{0.91}O_2$/CdS hybrid nanostructure hollow sphere system: the electrons in the conduction band of $Ti_{0.91}O_2$ recombine with holes in the valence band of CdS nanoparticles; then, the spectra-shifted emission emerges in this $Ti_{0.91}O_2$/CdS composite material.

To better study the charge transfer between present $Ti_{0.91}O_2$ nanosheets and CdS nanoparticles, transient time-resolved PL decay measurements were carried out on the samples excited at 266 nm. The PL decay curves can be well fitted to the biexponential function in the form of $f(t) = A_1 \exp(-t/\tau_1) + A_2 \exp(-t/\tau_2)$. The average lifetime τ is calculated by the form of $\tau = (A_1\tau_1^2 + A_2\tau_2^2)/(A_1\tau_1 + A_2\tau_2)$ and the all later lifetime calculations base on the form. Therefore, the average PL lifetime for $Ti_{0.91}O_2$ is 0.43 ns and the average PL lifetime for CdS is 0.35 ns as shown in Fig. 2b. More importantly, the average PL lifetime of $Ti_{0.91}O_2$/CdS hybrid structures is remarkably increased to 3.75 ns compared with the abovementioned PL lifetime of only $Ti_{0.91}O_2$ nanosheets or CdS nanoparticles. Based on the new type charge transfer mechanisms in $Ti_{0.91}O_2$/CdS hybrid interfaces, the electrons stay at the conduction band of $Ti_{0.91}O_2$ nanosheets, but the holes can either relax to the defect state levels or be transferred to the valence band levels of CdS nanoparticles. Due to the lower symmetry at the $Ti_{0.91}O_2$/CdS hybrid interface, the optical recombination from the electrons in the conduction band of $Ti_{0.91}O_2$ and the holes in the value band level of CdS causes prolonged PL lifetime. However, the experiment results also indicate weak optical activity of $Ti_{0.91}O_2$/CdS hollow sphere nanostructures under a 400-nm laser excitation and no obvious occurring of sensitization of CdS on $Ti_{0.91}O_2$. This means that the electrons in the conduction band of CdS would be inclined to recombination with hole in the value band of CdS rather than transfer to the conduction band of $Ti_{0.91}O_2$ nanosheets. These experiment results show that different from traditional type II fluorescence can be well explained by the new type II spatial separation of electrons and holes across the $Ti_{0.91}O_2$/CdS hybrid interface. Moreover, to better compare charge transfer and electronic interaction between $Ti_{0.91}O_2$/CdS and TiO_2/CdS, PL spectra and transient time-resolved PL decay measurements were carried out on the samples $Ti_{0.91}O_2$/CdS and TiO_2/CdS excited at 266 nm laser wavelength as shown in Additional file 1: Figure S3(a). Compared with TiO_2/CdS spheres, the emission peak of $Ti_{0.91}O_2$/CdS spheres show the same emission peak. However, the prolonged decay lifetime observed in $Ti_{0.91}O_2$/CdS hollow spheres reveals that decay dynamics for $Ti_{0.91}O_2$/CdS hollow spheres are fundamentally different from traditional TiO_2/CdS system.

To further investigate the interactive charge transfer mechanism between CdS and $Ti_{0.91}O_2$ hybrid structure, we compare the PL spectra and PL decay properties of hollow and solid $Ti_{0.91}O_2$/CdS hybrid spheres with 266 and 400 nm excitation, respectively. When $Ti_{0.91}O_2$/CdS is excited at 266 nm, the electrons ultimately stay at the conduction band of $Ti_{0.91}O_2$, and the holes can be transferred to the value band of CdS nanoparticles. The optical recombination between electrons in the conduction band of $Ti_{0.91}O_2$, and holes in the value band of CdS is allowed. However, the $Ti_{0.91}O_2$/CdS solid spheres contain the PMMA template and the PEI moiety; thus, these insulating organic surfactants hinder charge transport in the $Ti_{0.91}O_2$/CdS interface. Due to the electronic coupling between the CdS and $Ti_{0.91}O_2$ hybrid structure, the charge carrier mobility can be greatly enhanced by

removing the organic surfactants from the quantum dots (QDs) surface. The photoluminescence (PL) spectra and PL decay lifetime are shown in Fig. 3a, b, respectively. The PL peaks of $Ti_{0.91}O_2$/CdS solid spheres were red-shifted compared with $Ti_{0.91}O_2$/CdS hollow sphere, and the average PL lifetime is 4.25 ns (solid spheres) and 3.69 ns (hollow sphere), which implies the photoexcited holes in the valence band of $Ti_{0.91}O_2$ is more difficult to inject into the valence band of CdS in solid hybrid structures. The PMMA templates and PEI were completely eliminated to enhance inter-connectivity between alternating nanosheets of CdS and $Ti_{0.91}O_2$ and lead to an enhanced PL quenching phenomenon and shortened PL decay lifetime. Thus, the PL quenching effect in $Ti_{0.91}O_2$/CdS hybrid structures is attributed to the electrons dissociation because the bleach decay of the surface trapping does not explain the efficient PL quenching phenomenon. The charge separation process in $Ti_{0.91}O_2$/CdS hybrid structures occurs via the hole transfer from the valence band of $Ti_{0.91}O_2$ to the valence band of CdS nanocrystals based on the new type II indirect optical transition in a close-packed $Ti_{0.91}O_2$/CdS hybrid nanostructures. Thus, the carrier recombination lifetime by indirect optical transition has been decreased from 4.25 ns (solid sphere) to 3.69 ns (hollow sphere).

By tuning the excitation wavelengths to 400 nm at higher excitation power, the PL spectra and transient time-resolved PL decay dynamics were measured. The results show that the feeble PL spectra with 10 times integrated time are shown in Fig. 3c, and the average PL lifetime (0.59 ns) of $Ti_{0.91}O_2$/CdS solid hybrid structures is shorter than the PL lifetime (0.45 ns) of $Ti_{0.91}O_2$/CdS hollow hybrid structures as shown in Fig. 3d, suggesting that CdS has higher electron transfer rate toward $Ti_{0.91}O_2$ according to the traditional type II $Ti_{0.91}O_2$/CdS heterostructure. Compared with the case of 266 nm excitation, the shorter PL lifetime with 400 nm excitation indicates that PL quenching effect is further enhanced due to optical recombination between electrons and holes in the $Ti_{0.91}O_2$/CdS system or the wastage of holes for photocorrosion in the CdS nanoparticles. Therefore, the $Ti_{0.91}O_2$/CdS hollow hybrid spheres show weak optical activity under a 400-nm laser excitation, and no obvious sensitization emerges in the $Ti_{0.91}O_2$/CdS hybrid spheres.

To further investigate the charge carrier relaxation pathways in $Ti_{0.91}O_2$/CdS hollow hybrid interface, the excitation intensity-dependent PL spectra in the $Ti_{0.91}O_2$/CdS hybrid spherical structures were investigated under a 266-nm laser excitation. Under a 266-nm low-excitation intensity, we first observed that the 475 nm peak is dominant in the PL spectrum. With increasing the excitation

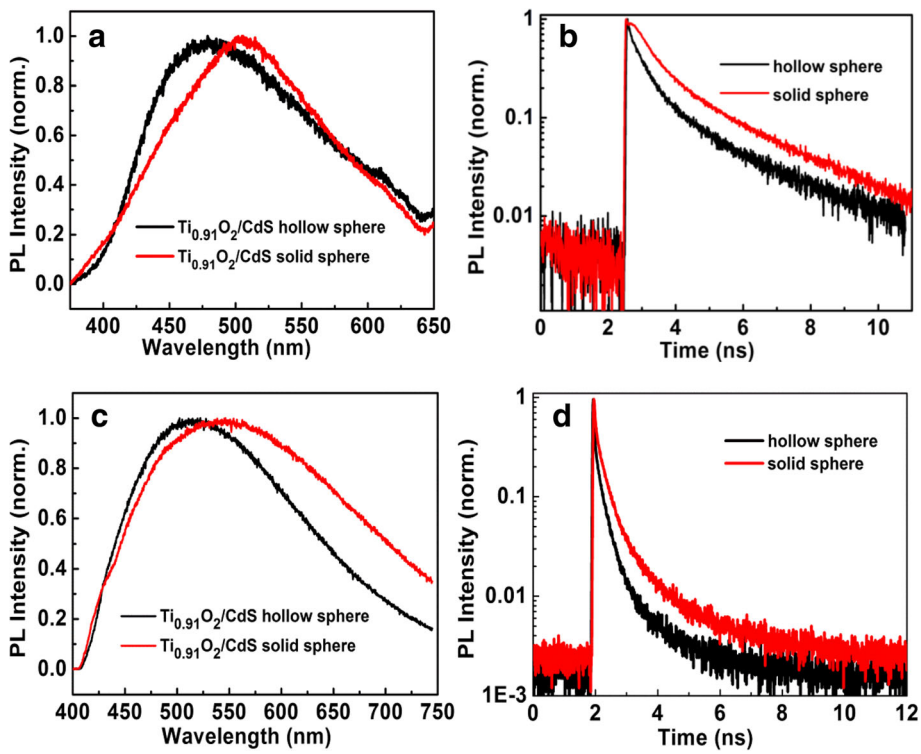

Fig. 3 **a** PL spectra of hollow $Ti_{0.91}O_2$/CdS (black) and solid $Ti_{0.91}O_2$/CdS (red) samples excited at 266 nm. **b** PL decay curves of hollow $Ti_{0.91}O_2$/CdS (black) and solid $Ti_{0.91}O_2$/CdS (red) samples with the 266 nm excitation. **c** PL spectra of hollow $Ti_{0.91}O_2$/CdS (black) and solid $Ti_{0.91}O_2$/CdS (red) samples excited at 400 nm. **d** PL decay curves of hollow $Ti_{0.91}O_2$/CdS (black) and solid $Ti_{0.91}O_2$/CdS (red) samples with the 400 nm excitation

power, the corresponding PL spectra intensity varied as a function of the excitation power ranging from 300 to 1000 W/cm^2 and the central peak wavelength of PL spectrum shift from 475 to 560 nm as shown in Fig. 4a. We tentatively attributed to electron transfer from conduction band of $Ti_{0.91}O_2$ to conduction band of CdS when $Ti_{0.91}O_2$/CdS hybrid nanostructures were excited by higher power 266 nm laser; then, the electron-hole recombination occurs between electrons in conduction band of CdS and holes in the valence band or the defect level of CdS nanoparticles according to type I recombination mechanism as shown in Fig. 4b. These varied PL spectra show that the red shift occurs with increasing excitation power. Such results confirm the different nature and origin of the emissions wavelength at 475 and 560 nm, respectively. Thus, the 475-nm emission wavelength indicates the type II emission property and the 560-nm emission wavelength reflects the type I emission property. The spectra shifted with excitation power indicate the competition mechanism between spatially direct and indirect recombination channels in $Ti_{0.91}O_2$/CdS composite interfaces. With the continuous by increasing the excitation power, more electrons with high-power excitation transfer from the conduction band of $Ti_{0.91}O_2$ to the conduction band of CdS nanoparticles, leading to a strongly increasing intensity ratio between central wavelength 560 and 475 nm, and the photoluminescence intensity ratio of two emission peaks can reach to 3.5 as shown in Fig. 4c. However, the weak photoluminescence intensity implies that the electron transfer from the conduction band of $Ti_{0.91}O_2$ to the conduction band of CdS nanoparticles only plays a minor role in the appearance of PL emission.

To further verify the two kinds of transition mechanisms with different excitation power in the $Ti_{0.91}O_2$/CdS hollow spheres, the probing wavelength-dependent time-resolved photoluminescence (TRPL) experiment was performed with different excitation power density. It is suitable to monitor the charge carrier transfer or electron-hole recombination process in the $Ti_{0.91}O_2$/CdS interface. The TRPL lifetimes of $Ti_{0.91}O_2$/CdS were measured with different probe wavelengths at 450, 500, and 550 nm, respectively. And the corresponding 450, 500, and 550 nm band-pass filter with a 10-nm bandwidth was used. The TRPL give longer decay lifetimes (3.72 ns) at shorter wavelength (450 nm) in the $Ti_{0.91}O_2$/CdS interface as shown in Fig. 4d because of the spatial separation of the charge carriers in the composite structures with the electrons in the conduction band of $Ti_{0.91}O_2$ nanosheets and holes in valence band of CdS nanoparticles. This type II hybrid structures reduce the PL intensity due to the smaller overlap between electron

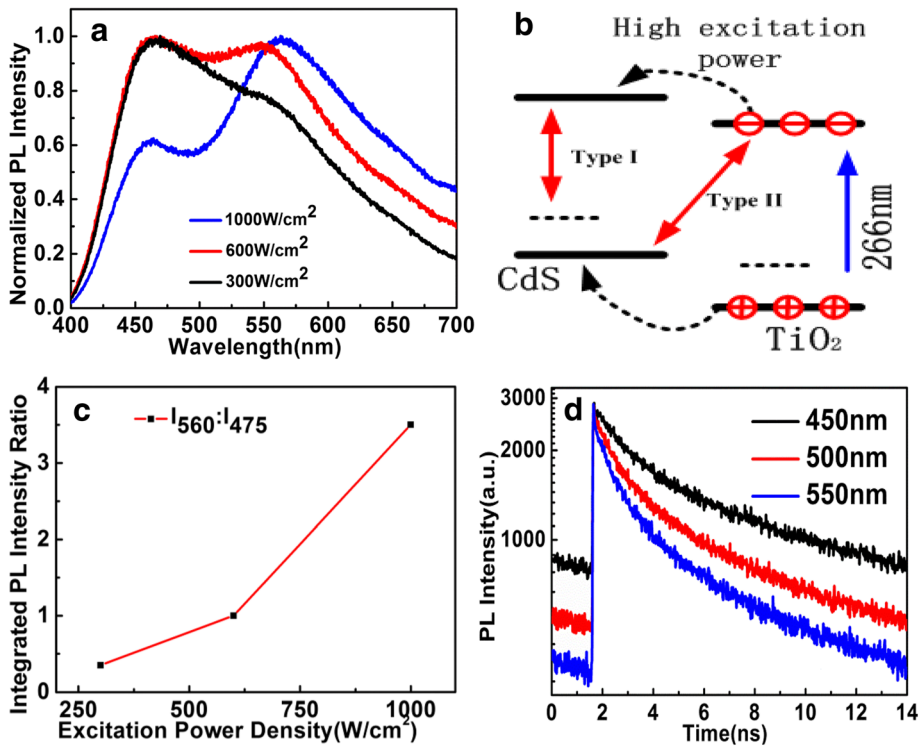

Fig. 4 **a** Excitation power dependence of PL spectra. **b** Electron transfer from conduction band of $Ti_{0.91}O_2$ to CdS with high-power excitation. **c** The integrated PL intensity ratio between central wavelength 560 and 475 nm. **d** The time-resolved PL measurements for 450, 500, and 550 nm with 266 nm excitation wavelength

and hole wave functions and consequently enhances PL recombination lifetimes. However, the PL lifetimes (1.61 ns) at longer wavelength (550 nm) become faster due to enhancing the wave function overlap between the electron of conduction band (CB) and hole of valence band (VB) in the CdS nanoparticles as shown in Fig. 4d. This findings clearly reveal that the photoexcited carriers in the $Ti_{0.91}O_2$/CdS make a significant contribution to the longer PL lifetimes. This evidence further confirms that the dominant PL is from the recombination between the electron in the CB of $Ti_{0.91}O_2$ and hole in the VB in of CdS nanoparticles. These findings confirm that electrons in the conduction band of $Ti_{0.91}O_2$ nanosheets recombine with holes in the valence band of CdS nanoparticles through indirect optical transition that is different from traditional TiO_2/CdS system. These prolonged carrier lifetime makes the $Ti_{0.91}O_2$/CdS composite nanostructure most suitable for photovoltaic applications. To characterize the ability of the synthetic samples, linear J –V curves were recorded as shown in Additional file 1: Figure S4. The great enhancement of the photocurrent after CdS sensitization shows the advantage of the $Ti_{0.91}O_2$/CdS compared to the $Ti_{0.91}O_2$ with light illumination. Therefore, a higher loading of the photosensitizer will lead to a higher photocurrent density.

Conclusions

In summary, we have detected novel indirect optical transition (IOT) properties in the multilayer PEI/$Ti_{0.91}O_2$/PEI/CdS hybrid nanostructures from the PL spectra and time-resolved PL measurements. From the PL spectral and TRPL measurement, the red-to-blue shift light emission emerges in this novel composite material. And prolonged photoluminescence lifetime of $Ti_{0.91}O_2$/CdS composite nanostructure compared with only $Ti_{0.91}O_2$ spheres or CdS nanoparticles was found. These results demonstrate new photoluminescence recombination mechanism due to the optical recombination between holes in the value band level of CdS and electrons in the conduction band level of $Ti_{0.91}O_2$ that is different from traditional TiO_2/CdS composite system. By tuning the excitation wavelengths and excitation power, the PL spectra and PL lifetimes of $Ti_{0.91}O_2$/CdS hybrid structures exhibit an excitation wavelength- and excitation power-dependent behavior. From the band-gap configurations, the IOT for $Ti_{0.91}O_2$/CdS hybrid structure which lead to prolonged carrier lifetime make for charge carrier separation and extraction for the important applications in photovoltaic system.

Additional file

Additional file 1: Optical measurement of alternating ultrathin $Ti_{0.91}O_2$ nanosheets and CdS nanoparticles hybrid spherical structures by the layer-by-layer assembly technique. (DOC 593 kb)

Abbreviations

IOT: Indirect optical transition; PL: Photoluminescence; PMMA: Polymethyl methacrylate; QDs: Quantum dots; TRPL: Time-resolved photoluminescence

Acknowledgements

We thank Wenguang Tu, Haijin Li, and Ping Li for the sample support and helpful discussions.

Funding

This work was supported by the National Science Foundation of China under grant nos. 61307067 and 11574125, Science Foundation of Shandong Province under grant no. ZR2015JL024, Taishan scholar project of Shandong Province under grant no. ts201511055, and Fundamental Research funds for the Central Universities under grant no. 30920130129625.

Availability of Data and Materials

The datasets generated during and/or analyzed during the current study are available from the corresponding authors on reasonable request.

Authors' Contributions

XQ and YC conceived and designed the experiments and co-wrote the manuscript. KL, ZM, and LM prepared the samples. JM, ZL, WD, and WH performed the optical experiments. XQ and YC co-wrote the manuscript. All authors read and approved the final manuscript.

Competing Interests

The authors declare that they have no competing interests.

Publisher's Note

Received: 24 November 2017 Accepted: 27 February 2018
Published online: 07 March 2018

References

1. Linsebigler AL, Lu GQ, Yates YT (1995) Photocatalysis on TiO_2 surfaces: principles, mechanisms, and selected results. Chem Rev 95:735–758
2. Brown GE, Henrich VE, Casey WH, Clark DL, Eggleston C, Femly A, Goodman DW, Gratzel M, Macial G, McGarthy MI, Nealson KH, Sverjensky DA, Toney MF, Zachara JM (1999) Metal oxide surfaces and their interactions with aqueous solutions and microbial organisms. Chem Rev 99(1):77–174
3. Bilmes SA, Mandelbaum P, Alvarez F, Victoria NM (2000) Surface and electronic structure of titanium dioxide photocatalysts. J Phys Chem B 104(42):9851–9858
4. Li L, Yang X, Gao J, Tian HN, Zhao JZ, Hagfeldt A (2011) Highly efficient CdS quantum dot-sensitized solar cells based on a modified polysulfide electrolyte. J Am Chem Soc 133(22):8458–8460
5. Anikeeva PO, Halpert JE, Bawendi MG, Bulovic V (2009) Quantum dot light-emitting devices with electroluminescence tunable over the entire visible spectrum. Nano Lett 9(7):2532–2536
6. Caruge JM, Halpert JE, Wood V, Bulovic V, Bawendi MG (2008) Colloidal quantum-dot light-emitting diodes with metal-oxide charge transport layers. Nat Photonics 2(4):247–250
7. Chan Y, Caruge JM, Snee PT, Bawendi MG (2004) Multiexcitonic two-state lasing in a CdSe nanocrystal laser. Appl Phys Lett 85(13):2460–2462
8. Klimov VI, Ivanov SA, Nanda J, Achermann M, Bezel I, McGuire JA, Piryatinski A (2007) Single-exciton optical gain in semiconductor nanocrystals. Nature 447(7143):441–446
9. Klimov VI, Mikhailovsky AA, Xu S, Malko A, Hollingsworth JA, Leatherdale CA, Eisler HJ, Bawendi MG (2000) Optical gain and stimulated emission in nanocrystal quantum dots. Science 290(5490):314–317
10. Lee YL, Chi CF, Liau SY (2009) CdS/CdSe co-sensitized TiO_2 photoelectrode for efficient hydrogen generation in a photoelectrochemical cell. Chem Mater 22(3):922–927
11. Sun B, Marx E, Greenham NC (2003) Photovoltaic devices using blends of branched CdSe nanoparticles and conjugated polymers. Nano Lett 3(7):961–963
12. Vempati S, Celebioglu A, Uyar T (2015) Defect related emission versus intersystem crossing: blue emitting ZnO/graphene oxide quantum dots. Nano 7(38):16110–16118

13. Stinaff EA, Scheibner M, Bracker AS, Ponomarev IV, Korenev VL, Ware ME, Doty MF, Reinecke TL, Gammon D (2006) Optical signatures of coupled quantum dots. Science 311(5761):636–639
14. Robel I, Subramanian V, Kuno M, Kamat PV (2006) Quantum dot solar cells. Harvesting light energy with CdSe nanocrystals molecularly linked to mesoscopic TiO_2 films. J Am Chem Soc 128(7):2385–2393
15. Kongkanand A, Tvrdy K, Takechi K, Kuno M, Kamat PV (2008) Quantum dot solar cells. Tuning photoresponse through size and shape control of CdSe –TiO_2 architecture. J Am Chem Soc 130(12):4007–4015
16. Zhang XJ,Lin SW, Liao JJ, Pan NQ, Li DH, Cao XK, Li JB (2013)Uniform deposition of water-soluble CdS quantum dots on TiO2 nanotube arrays by cyclic voltammetric electrodeposition: effectively prevent aggregation and enhance visible-light photocatalytic activity. Electrochimica Acta 108:296–303
17. Biswas S, Hossain MF, Takahashi T, Kubota Y (2008) Comparative study of photocatalytic activity in CdS-TiO_2 thin films prepared by two different techniques. J Vac Sci Tech A 26(4):1002–1006
18. Piris J, Ferguson AJ, Blackburn JL, Norman AG, Rumbles G, Selmarten DC, Kopidakis N (2008) Efficient photoinduced charge injection from chemical bath deposited CdS into mesoporous TiO_2 probed with time-resolved microwave conductivity. J Phys Chem C 112(20):7742–7749
19. Robert D (2007) Photosensitization of TiO_2 by M_xO_y and M_xS_y nanoparticles for heterogeneous photocatalysis applications. Catal Today 122(1):20–26
20. Jia HM, Xu H, Hu Y, Tang YW, Zhang LZ (2007) TiO_2@ CdS core-shell nanorods films: fabrication and dramatically enhanced photoelectrochemical properties. Electrochem Commun 9(3):354–360
21. Baron R, Huang CH, Bassani DM, Onopriyenko A, Zayats M, Willner I (2005) Hydroge-bonded CdS nanoparticle assemblies on electrodes for photoelectrochemical applications. Angew Chem Int Ed 117(26):4078–4083
22. Lee YL, Lo YS (2009) Highly efficient quantum-dot-sensitized solar cell based on co-sensitization of CdS/CdSe. Adv Funct Mater 19(4):604–609
23. Kukovecz Á, Hodos M, Kónya Z, Kiricsi I (2005) Complex-assisted one-step synthesis of ion-exchangeable titanate nanotubes decorated with CdS nanoparticles. Chem Phys Lett 411(4):445–449
24. Xiao MW, Wang LS, Wu YD, Huang XJ, Dang Z (2007) Preparation and characterization of CdS nanoparticles decorated into titanate nanotubes and their photocatalytic properties. Nanotech 19(1):015706
25. Zhang YJ, Yan W, Wu YP, Wang ZH (2008) Synthesis of TiO_2 nanotubes coupled with CdS nanoparticles and production of hydrogen by photocatalytic water decomposition. Mater Lett 62(23):3846–3848
26. Das K, De SK (2009) Optical properties of the type-II core–shell TiO_2@ CdS nanorods for photovoltaic applications. J Phys Chem C 113(9):3494–3501
27. Tu W, Zhou Y, Feng SC, Xu QF, Li P, Wang XY, Xiao M, Zou ZG (2015) Hollow spheres consisting of $Ti_{0.91}O_2$/CdS nanohybrids for CO_2 photofixation. Chem Commun 51(69):13354–13357